Geophysical Research Letters

RESEARCH LETTER
10.1029/2019GL085361

Convection-Diffusion Competition Within Mixed Layers of Stratified Natural Waters

Oscar Sepúlveda Steiner[1], Damien Bouffard[2], and Alfred Wüest[1,2]

[1]Physics of Aquatic Systems Laboratory, Margaretha Kamprad Chair, Institute of Environmental Engineering, École Polytechnique Fédérale de Lausanne, Lausanne, Switzerland, [2]Department of Surface Waters–Research and Management, Eawag, Swiss Federal Institute of Aquatic Science and Technology, Kastanienbaum, Switzerland

Key Points:
- Mixed layers often develop in natural waters under simultaneous influence of convectively driven and shear-induced mixing
- Microstructure measurements and a diffusive-shape model were used to evaluate effects of turbulence adjacent to convective mixed layers
- A Péclet number parameterization allows for estimation of bulk turbulent quantities given the shape of mixed layers

Supporting Information:
- Supporting Information S1

Correspondence to:
O. Sepúlveda Steiner,
oscar.sepulvedasteiner@epfl.ch

Citation:
Sepúlveda Steiner, O., Bouffard, D., & Wüest, A. (2019). Convection-diffusion competition within mixed layers of stratified natural waters. *Geophysical Research Letters*, *46*. https://doi.org/10.1029/2019GL085361

Received 12 SEP 2019
Accepted 2 NOV 2019
Accepted article online 9 NOV 2019

Abstract In stratified natural waters, convective processes tend to form nearly homogeneous mixed layers. However, shear-driven turbulence generated by large-scale background flow often rapidly smooths them through mixing with the stratified surroundings. Here we studied the effect of background turbulence on convectively driven mixed layers for the case of bioconvection in Lake Cadagno, Switzerland. Along with microstructure measurements, a diffusive-shape model for the mixed layers allowed us to define (i) mixed layer thickness and (ii) diffusive transition length. Further microstructure analysis was performed allowing estimation of convective turbulence in the mixed layer and shear-driven turbulence quantified by eddy diffusion in their surroundings. Based upon these results, we propose a Péclet number scaling that relates mixed layer shape to the opposing effects of convection and diffusion. We further validate this quantitative approach by applying it to two other distinct convective systems representative of double-diffusive convection and radiatively driven under-ice convection.

Plain Language Summary In natural waters with density stratification, convection and diffusion are generated by different mechanisms and induce different mixing effects. Convection is driven by local instabilities in the density profile, whereas enhanced diffusion is due to turbulence generated by large-scale circulation. These processes can occur simultaneously in the case of convectively driven mixed layers, which are smoothed by turbulent diffusion. Mixed layers can also be created by a specific biophysical interaction: bioconvection. A community of motile and heavy bacteria that accumulate at a specific depth in Lake Cadagno, Switzerland, drives bioconvection and is able to create homogeneous layers of up to 1 m thickness. Using a combination of high-resolution temperature measurements along with a mixed layer model, we propose an empirical relation between this layer shape and the different mixing effects from convection and diffusion. We also relate mixed layer shape to turbulence estimates for other types of convection in natural waters.

1. Introduction

Convective turbulence and eddy diffusion are key concepts for quantifying mixing in natural waters. Both processes often occur simultaneously; however, separating their contribution to mixing in stratified systems remains a challenge. Interactions of these processes can augment or limit mixing. Shear-induced bottom boundary convection (Lorke et al., 2005; Moum et al., 2004) provides an example of positive feedback. In this case, large-scale currents interact with a sloping bathymetry to generate shear instabilities which drive convection and mix bottom layers. The limiting effect occurs, for example, in the classic case of cooling-induced surface convection (Imberger, 1985; Shay & Gregg, 1986). This interaction consists of a surface mixed layer formed during nighttime cooling which has to overcome smoothing effects of wind-driven entrainment and can be characterized by the Monin-Obukhov length (Lombardo & Gregg, 1989; Tedford et al., 2014). In the present study, we focus on the limiting effect and refer to it as competition.

In lakes, where background turbulence is weaker than that observed in the ocean (Wüest et al., 2000), a variety of convective processes can develop within different, stably stratified sections of the water column (Bouffard & Wüest, 2019). These can induce formation of almost homogeneous mixed layers (hereafter referred to as MLs). Typical examples include double-diffusive convection (Huppert & Turner, 1972; Sommer, Carpenter, Schmid, Lueck, Schurter, & Wüest, 2013), radiatively driven under-ice convection (Bouffard et al., 2016; Kirillin et al., 2012; Yang et al., 2017), thermobaric convection (Crawford & Collier,

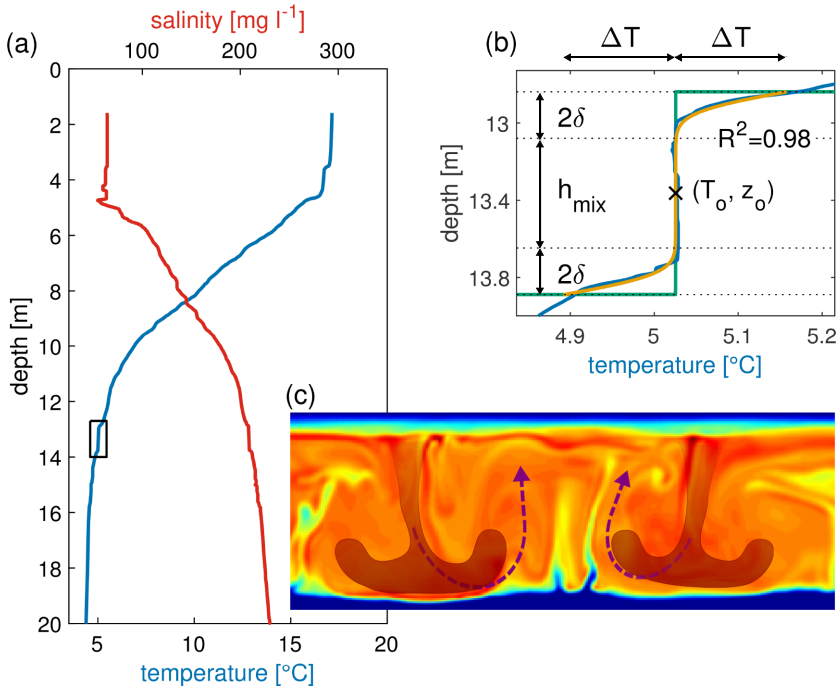

Figure 1. Water column profile and ML structure of Lake Cadagno. (a) Temperature (blue) and salinity (red) profiles measured on 12 July 2017 at 15:30. (b) Enlargement of the black box region in (a) showing the ML temperature profile (blue) with its respective fitting of the ML model (orange), initial step-like ML (green) and the definition of h_{mix} and δ interpreted in this study. R^2 is the coefficient of determination indicating goodness of fit. (c) Snapshot of bacteria-driven convective plumes that generate MLs in Lake Cadagno. Color map corresponds to relative bacteria concentration (−) resulting from Direct Numerical Simulations (DNS; courtesy of George Constantinescu and Tobias Sommer).

1997; Schmid et al., 2008), and bioconvection (Sommer et al., 2017). Yet, large-scale flows of surrounding stratified waters generate shear-induced turbulence (Bouffard et al., 2012; Saggio & Imberger, 2001) usually quantified by eddy diffusion, which can smooth out those MLs (Figure S1 in the supporting information). A better understanding of convection and turbulent diffusion interaction can help elucidate the role of background turbulence in the maintenance of convective MLs.

We investigated bioconvective MLs to this end. Bioconvection is a process in which dense and motile organisms change the density of their fluid environment triggering hydrodynamic instabilities. Initially observed in laboratory experiments, this phenomenon was recently detected in natural waters by Sommer et al. (2017) who describe a high concentration of dense and motile bacteria inducing formation of MLs in Lake Cadagno, Switzerland (Figure 1). The bioconvective MLs of Lake Cadagno are an exemplary case for studying convection-diffusion competition because wind-induced shearing is weak in the interior (Figure S2). This enables the bacteria to develop well-defined and persistent MLs (Figures 1b and S2a, respectively).

In this paper, we analyzed vertical profiles of bacteria-induced convective MLs from six field campaigns conducted on Lake Cadagno. The analysis used microstructure measurements of the water column complemented with a diffusive-shape model that characterizes the effect of background turbulence on the MLs. This approach allows us to relate ML profile shapes to eddy diffusion acting against convective mixing by using a Péclet number scaling. These findings can be generalized by applying the scaling to MLs resulting from double-diffusive and under-ice convection in natural water environments.

2. Measurements and Methods

2.1. Study Site and Field Campaigns

This study was conducted on the alpine meromictic Lake Cadagno (46° 33′ 3.13″ N, 8° 42′ 41.51″ E, 1,920 m asl, max. depth of 21 m and surface area of 0.26 km^2). Lake Cadagno is permanently stratified exhibiting an oxygen-rich upper layer (top ~10 m) and an anoxic and sulfide-rich deep-water layer (deepest ~10 m). During

Table 1
Characteristics of Observed Convective MLs in Lake Cadagno for Each of the Six Field Campaigns

Parameter	Units	July 2016[a]	August 2016	July 2017	August 2017a	August 2017b	August 2018
Thickness of mixed layer (h_{mix})[b]	m	0.83 ± 0.28 (26)	0.75 ± 0.35 (38)	0.67 ± 0.30 (63)	0.66 ± 0.34 (85)	0.37 ± 0.11 (24)	0.50 ± 0.22 (136)
Diffusive length (δ)[b]	m	0.09 ± 0.05 (26)	0.06 ± 0.04 (38)	0.17 ± 0.11 (63)	0.15 ± 0.09 (85)	0.14 ± 0.05 (24)	0.18 ± 0.09 (136)
Background stability (N_B^2)[b]	10^{-5} s^{-2}	10.1 ± 1.8 (26)	11.6 ± 1.9 (38)	16.2 ± 4.0 (63)	11.5 ± 2.6 (85)	12.3 ± 2.5 (24)	7.9 ± 1.5 (136)
Mixed layer dissipation rate (ε_{ML})[c]	10^{-10} W kg^{-1}	4.5 ⟨1.9⟩ (26)	4.1 ⟨1.2⟩ (38)	14.5 ⟨3.9⟩ (61)	10.6 ⟨2.7⟩ (85)	3.1 ⟨1.9⟩ (24)	4.3 ⟨2.7⟩ (130)
Background dissipation rate (ε_B)[c]	10^{-10} W kg^{-1}	5.7 ⟨1.1⟩ (26)	29.6 ⟨3.1⟩ (38)	34.1 ⟨3.0⟩ (63)	24.6 ⟨2.0⟩ (85)	8.6 ⟨1.0⟩ (24)	17.5 ⟨2.2⟩ (136)
Background diffusivity (K_B)[c]	10^{-6} m^2 s^{-1}	1.0 ⟨0.8⟩ (26)	3.4 ⟨2.1⟩ (38)	3.4 ⟨2.5⟩ (63)	3.4 ⟨1.6⟩ (85)	1.2 ⟨0.7⟩ (24)	2.8 ⟨1.3⟩ (136)
Convective plume velocity (w_*)[b]	10^{-3} m s^{-1}	0.49 ± 0.40 (26)	0.48 ± 0.25 (38)	0.55 ± 0.59 (61)	0.56 ± 0.50 (85)	0.33 ± 0.25 (24)	0.37 ± 0.25 (130)

[a]Data from this field campaign was also presented in Sommer et al. (2017). Although the analysis is similar, the results are independent and according to the methods presented herein. [b]Results are reported as arithmetic mean ± standard deviation and the number of samples in parentheses. [c]Statistics of the rate of dissipation and diffusivity are reported following Baker and Gibson (1987) given by the mle-mean for a lognormal distribution accompanied by its intermittency factor (σ^2_{mle}) inside pointy brackets and the number of samples in parentheses.

summer, the phototrophic, heavy, and motile bacteria *Chromatium okenii* find ideal conditions for their metabolism at the oxic-anoxic transition zone (Schanz et al., 1998), where they accumulate at high concentrations. The oxycline limits their vertical extent, as anoxic conditions are necessary to perform anoxygenic photosynthesis, their main metabolic process. Upward migration of these heavy bacteria (density ~1,150 kg m^{-3}) leads to an upward density flux, which in turn causes density instability of the fluid and initiation of convective mixing. This process forms MLs of temperature and salinity (Figure 1).

To resolve the vertical shape and estimate turbulent parameters for the MLs, we measured temperature and conductivity at high resolution with a VMP-500 (Rockland Scientific International, Canada) free-falling vertical microstructure profiler. The profiler is equipped with two fast FP07 thermistors and two fast SBE-7 conductivity microsensors mounted at the nose of the instrument sampling at frequencies of 512 Hz. The sinking speed of the profiler was set between 0.10 and 0.20 m s^{-1}. Sommer, Carpenter, Schmid, Lueck, and Wüest (2013) provides detailed description of the VMP-500 and its sensors. Continuous measurements (from 8 to 48 hr duration with intervals of 20 to 30 min between profiles) were performed during the summers of 2016, 2017, and 2018 (Table 1).

2.2. Diffusive-Shape Mixed Layer Model

A model was developed to interpret measured ML temperature profiles. The specific objectives of the model were to (i) properly define ML thickness (h_{mix}) and (ii) define the extent of the upper and lower ML boundaries affected by the vertical diffusivity which generates a smooth transition to background stratification (2δ in Figure 1b). The mixed layer model (Φ_T) is derived from the 1-D vertical diffusion equation given a step function (i.e., fully convective ML) with height h and temperature T_o as initial conditions (green line in Figure 1b). The equation is subject to Dirichlet boundary conditions at the top (T_{top}) and bottom (T_{bottom}) of the domain. An analytical solution can be derived by applying the superposition method to recover the boundary conditions. In this paper, we focus on symmetric MLs, whereas the nonsymmetric case is presented in Text S1 and Figure S3. Given a symmetric temperature step function ($\Delta T = T_o - T_{bottom} = -T_o + T_{top}$) and limited time-scales (with respect to the diffusive time scale), the solution is expressed as

$$\Phi_T(z) = \Delta T\left[\mathrm{erf}\left(\frac{\frac{h}{2}-(z-z_o)}{\delta}\right)-\mathrm{erf}\left(\frac{\frac{h}{2}+(z-z_o)}{\delta}\right)\right]+T_o, \quad (1)$$

where z is positive downward and z_o is the center of the ML position, $\delta = \sqrt{4K\tau}$ is the diffusive length with K expressing diffusivity, and τ the diffusive time scale ($\tau = \delta^2/4K$). Consequently, τ is the elapsed time since

complete homogenization of the ML (step-like function) and the measured temperature profile. The ML thickness h_{mix} is then given by

$$h_{\mathrm{mix}} = h - 4\delta. \tag{2}$$

Fitting the measured profiles to Φ_T provides information about the background diffusivity affecting the ML shape at the time of measurement. Lower δ values relate to high convective activity relative to diffusivity, whereas higher δ values suggest weak convection relative to background turbulence.

Finally, including a ML slope (G_T) improves the goodness of fit for cases exhibiting enhanced turbulence within h_{mix}. For well-defined MLs, G_T reaches values close to zero, without affecting the procedure. The final ML model reads

$$\Phi_T(z) = \Delta T\left[\mathrm{erf}\left(\frac{\frac{h}{2} - (z - z_o)}{\delta}\right) - \mathrm{erf}\left(\frac{\frac{h}{2} + (z - z_o)}{\delta}\right)\right] + T_o - G_T(z - z_o). \tag{3}$$

2.3. Data Analysis

2.3.1. Physicochemical Characteristics and Water Column Stability

Temperature and conductivity microstructure values were adjusted against CTD data obtained from Sea-Bird SBE-3F and SBE-4C sensors (sampled at 64 Hz) installed on the VMP-500. We use the water ionic composition of Lake Cadagno (Uhde, 1992) to calculate salinity and density from the CTD-adjusted corrected temperature and conductivity microstructure profiles. This density estimate corresponds to the density of water without bacteria. Finally, $N^2 = \frac{g}{\rho_o}\frac{\partial \rho}{\partial z}$ accounts for the stability of the water column, where $g = 9.81$ m s^{-2} and $\rho_o = 1{,}000$ kg m^{-3}. N^2 is obtained in vertical segments of interest by linear fitting of the density $\rho(z)$ profiles over those segments.

2.3.2. Mixed Layer Model Fitting

A bounded nonlinear method was used to fit the CTD-adjusted temperature microstructure profiles and obtain the ML model (Φ_T) parameters. This approach allows h_{mix} and δ estimates characterizing the convective ML and diffusive region, respectively, for each profile collected on the six field campaigns (Table 1). Further details on initial values and boundary conditions for the fitting method are provided in Table S1. After fitting, only Φ_T with a $R^2 > 0.75$ and a ML thickness $h_{\mathrm{mix}} > 0.2$ m were considered for further analysis.

2.3.3. Dissipation Rate Estimates

We used temperature microstructure profiles to estimate rates of turbulent kinetic energy dissipation ε (W kg^{-1}) by adjusting the theoretical Batchelor (1959) spectrum to measured spectra of temperature gradients. This procedure used the maximum likelihood spectral fitting method (Ruddick et al., 2000) complemented with the Steinbuck et al. (2009) correction to calculate the smoothing rate of temperature variance χ_θ (°C^2 s^{-1}).

Dissipation in the ML ($\varepsilon_{\mathrm{ML}}$) was estimated by applying the method to the microstructure segment defined by h_{mix} resulting from Φ_T curve fitting. The section was divided into three subsegments with 50% overlap. Temperature gradient spectra of these segments were calculated, averaged, and then treated with the Batchelor fitting to estimate $\varepsilon_{\mathrm{ML}}$. Background dissipation (ε_{B}) was estimated in a similar way from segments of 1.5 m above and below h_{mix}, which were also divided into three subsegments with 50% overlap. A sensitivity analysis justifying the choice of 1.5 m segment lengths is presented in Figure S4.

2.3.4. Buoyancy Flux and Convective Quantities

Buoyancy flux (J_{b}) represents a key parameter for characterizing convective MLs. To estimate J_{b}, we use bioconvection DNS results reported by Sommer et al. (2017). These showed that for a constant upward bacterial migration speed and background stratification, the modeled ML reached a steady state with a ratio between dissipated (ε) and bacteria-produced (R) energies of $\varepsilon/R = 0.45$. These parameters give a bioconvective mixing efficiency of $\eta_{\mathrm{bC}} = 0.55$. In this study, the buoyancy flux in the ML is then calculated as

$$J_{\mathrm{b}}^{\mathrm{ML}} = \eta_{\mathrm{bC}}\, \varepsilon_{\mathrm{ML}} \tag{4}$$

Subsequently, the vertical convective velocity (w_*) can be characterized by

$$w_* = \left(J_b^{ML} \ell\right)^{1/3}, \tag{5}$$

where ℓ is a convective length scale. In this study we considered two independent estimates of ℓ: (i) $\ell = h_{mix}$ as obtained from the ML model fitting and (ii) $\ell \approx L_T$ with L_T defined as the Thorpe (1977) scale of overturns within h_{mix}. L_T is calculated using temperature microstructure data only (Dillon, 1982). The purpose of the second estimate is to further validate results obtained using bulk estimations (i.e., the ML model) by means of instantaneous microstructure properties.

2.3.5. Mixing and Transport

The influence of diapycnal mixing on the ML background (B) is accounted for by turbulent diffusivity following the Osborn (1980) model:

$$K_B = \Gamma \frac{\varepsilon_B}{N_B^2}, \tag{6}$$

where ε_B is the background dissipation rate and N_B^2 is the background stability. N_B^2 is obtained from linear fitting over 1.5 m long segments above and below the ML. Here we use a diapycnal mixing coefficient of $\Gamma = 0.15$, which is well suited for small to medium size lakes (Wüest et al., 2000).

Given the two transport processes involved in our ML analysis, the following Péclet number

$$Pe = \frac{w_* \ell}{K_B} \tag{7}$$

can be defined to compare the intensity of convection in the ML with background turbulent diffusion. Finally, to characterize the background energy regime, we use the buoyancy Reynolds number (Gibson, 1980):

$$Re_b = \frac{\varepsilon_B}{\nu N_B^2}, \tag{8}$$

with $\nu = 1.5 \times 10^{-6}$ m^2 s^{-1} (water temperature ~5 °C; Figure 1). Re_b defines three energy regimes (Ivey et al., 2008): molecular ($Re_b < 7$), transitional ($7 < Re_b < 100$), and turbulent ($Re_b > 100$).

3. Results

3.1. Mixed Layer Model Fitting

We acquired 336 VMP-500 profiles during six field campaigns (Table 1). Each profile reports duplicates of microstructure measurements (two FP07 sensors) for a total of 672 temperature profiles. Of these, 372 profiles (55.4%) passed the Φ_T fitting test with $R^2 > 0.75$ and $h_{mix} > 0.2$ m, and 39% (145 profiles) were measured during nighttime. Field campaigns thus detected numerous well-defined MLs and revealed their persistent presence during the entire day-night cycle.

Figure 2a summarizes ML model fitting results. Arithmetic means were 0.15 ± 0.09 m for δ and 0.61 ± 0.30 m for h_{mix}. Table 1 lists details of δ and h_{mix} for each of the six field campaigns. The July 2017 and August 2017a field campaigns were representative of the average values obtained for the entire data set.

3.2. Turbulent Quantities

Distributions of ML (ε_{ML}) and background (ε_B) dissipation rates (Figure 2b) appear lognormal. However, both are negatively skewed, presenting extreme values for $\varepsilon > 10^{-8}$ W kg^{-1}. Moreover, the kurtosis of the log-data is larger than the expected value of 3 (4.8 and 4.3 for ε_{ML} and ε_B, respectively). To reduce the weight of extreme values, the maximum likelihood estimator (mle) of a lognormal distribution was used to estimate means accompanied by their respective intermittency factor $\langle \sigma_{mle}^2 \rangle$ (Baker & Gibson, 1987). This approach gives an ε_{ML} mle-mean of 6.7×10^{-10} W kg^{-1} $\langle 2.7 \rangle$ and an ε_B mle-mean of 2.0×10^{-9} W kg^{-1} $\langle 2.3 \rangle$, indicating a generally weak turbulent regime with slightly more energetic turbulence outside the MLs.

The background diffusivity (K_B) distribution (not shown) also appears log-normal (log-data kurtosis of 5.0), with a resulting mle-mean of 2.8×10^{-6} m^2 s^{-1} $\langle 1.6 \rangle$. This value is in good agreement with the vertical

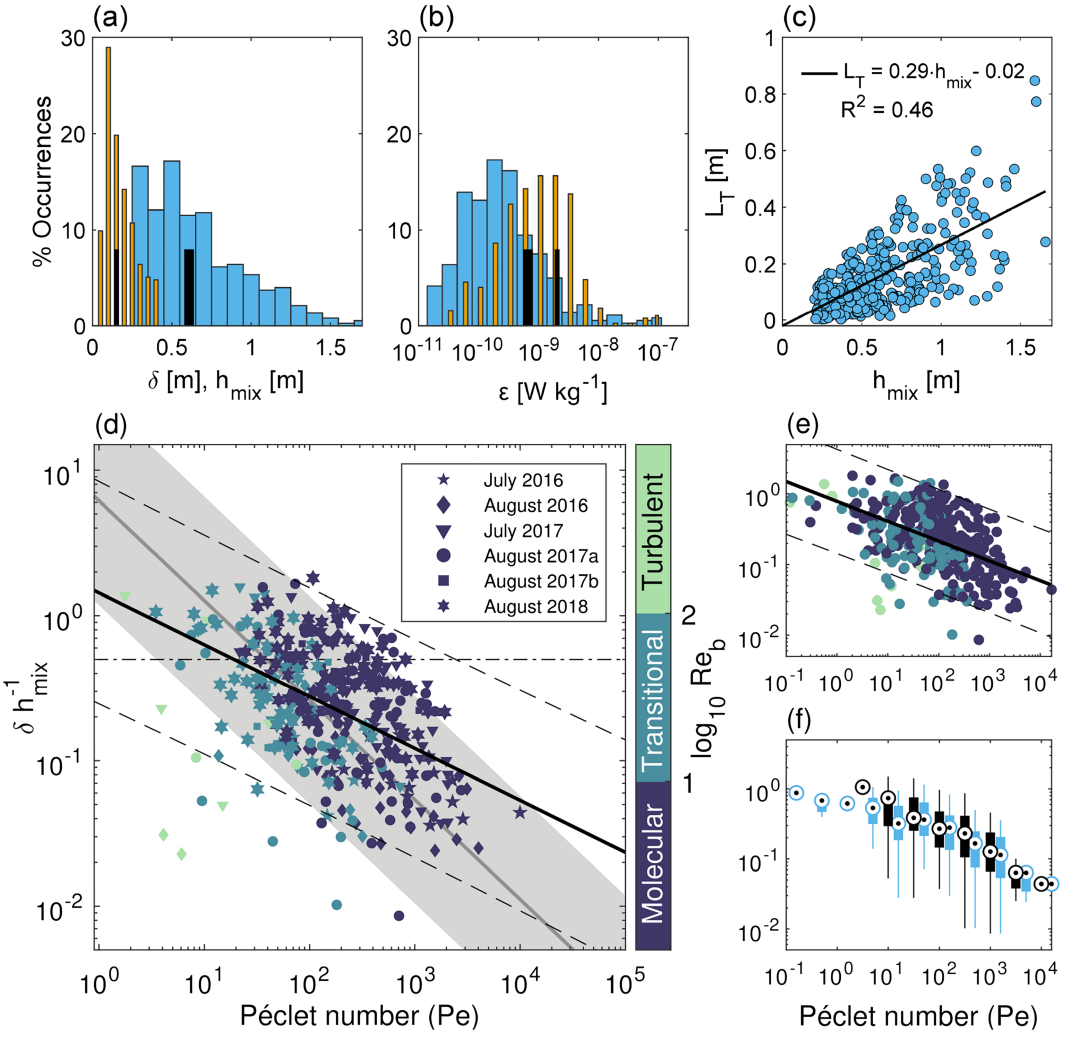

Figure 2. Distribution of ML model fitting and microstructure analysis results accompanied with a comparison of convection and diffusion. (a) Histograms of mixed layer thickness (h_{mix}; blue) and diffusive length (δ; orange). Thick and thin black bars represent arithmetic means for h_{mix} and δ, respectively. (b) Histogram of dissipation rates of turbulent kinetic energy in the MLs (ε_{ML}; blue) and background (ε_B; orange). Thick and thin black bars represent mle-means for ε_{ML} and ε_B, respectively. (c) Comparison of h_{mix} with Thorpe scales (L_T) within the MLs, black line represent best linear fit. (d) Geometrical ratio δh_{mix}^{-1} for convective MLs as a function of h_{mix}-based Péclet number (Pe). The blue to green color bar represents the three different background energy regimes defined by Re_b. For simplicity, we use $Re_b = 10$ as the limit between the molecular and transitional regime. The thick black line is the best fit for molecular and transitional regimes only (thin dashed lines, 95% confidence interval). Gray line and shade represent best fit and 95% confidence interval, respectively, when considering a constant diffusivity (K_{W94}) for the Pe calculation. The horizontal dot-dashed line indicates $\delta h_{mix}^{-1} = 0.5$. (e) Analogous to (d) for L_T-based Pe with $\hbar = 3L_T$. The thick black line and the thin dashed lines represent the best fit and its 95% confidence interval, respectively. (f) Boxplot of δh_{mix}^{-1} versus Pe for (d) in black and (e) in light blue. Dotted white circles represent median estimate of δh_{mix}^{-1} for half-decade bins of Pe. Vertical bars and lines represent the 25th and 75th percentiles.

diffusivity $K_{W94} = 1.6 \times 10^{-6}$ m^2 s^{-1}, which resulted from a tracer release experiment at the same depth in Lake Cadagno (Wüest, 1994).

Analysis of Thorpe scales of overturns showed an arithmetic mean of 0.14 ± 0.13 m. Moreover, when compared to h_{mix} (Figure 2c), the data follow a linear trend $L_T = 0.29h_{mix}$-0.02 ($R^2 = 0.46$; slope 95 % confidence interval of ±0.03). This result depicts a relation close to $h_{mix} \cong 3L_T$, which has also been reported for MLs formed by triple-diffusion convection (Sánchez & Roget, 2007). For further analysis, we thus consider $\hbar = 3$

L_T. Considering fully developed MLs from bioconvection DNS (Sommer et al., 2017; Figure 1c) and applying the ML model fitting along the whole lateral domain (>500 profiles) yields $L_T = 0.20 \pm 0.01$ m and $L_T\, h_{mix}^{-1} = 0.43 \pm 0.02$.

3.3. Convection-Diffusion Competition

A twofold comparison of the δh_{mix}^{-1} ratio versus the Péclet number (Pe; Figures 2d–2f) depicts opposing effects of convection and diffusion. High Pe values and low δh_{mix}^{-1} values generally indicate that background diffusivity does not significantly influence convective MLs. Low Pe values and high δh_{mix}^{-1} values on the other hand denote MLs subject to the smoothing effect of background diffusivity.

The data set also reveals more specific aspects of the interaction between convection and diffusion. Considering $\hbar = h_{mix}$, cases in which convection occurred almost without the influence of background diffusivity were characterized by $Pe > 10^3$ (Figure 2d). Moreover, all these cases occur in a background molecular regime and with a δh_{mix}^{-1} ratio less than 0.50. Diffusivity-influenced MLs (i.e., $\delta h_{mix}^{-1} > 0.50$) were encountered throughout the six campaigns and represent 23% of the data set. These have Pe values ranging from 10^1 to 10^3. The majority of profiles that meet the Φ_T fitting criteria develops in molecular-to-transitional energy regimes ($Re_b < 100$). Although 10 profiles show MLs with a turbulent background, these profiles represent only 3% of the data set. In cases representing molecular and transitional regimes only, the data follow a power law (black line, Figure 2d):

$$\delta h_{mix}^{-1} = 1.5 Pe^{-0.36}, \tag{9}$$

that relates the interplay of convection and diffusion to the ML shape. The results from Figure 2d show a relatively large degree of scatter within a 95% confidence interval and indicate an uncertainty up to $O(1)$ for Pe. For constant diffusivity (e.g., 1.6×10^{-6} m^2 s^{-1}; Wüest, 1994), the data points are well aligned with a power law $\delta h_{mix}^{-1} = 6.0 Pe^{-0.68}$ (gray line, Figure 2d) and show a smaller spread (gray area, Figure 2d). The large scatter when considering varying diffusivities in Figure 2d reflects the intrinsic variability (intermittency) of instantaneous microstructure-based turbulent estimates (Figure 2b).

An axis-independent analysis can be performed by using a L_T-based Péclet number (Pe_{L_T}) with $\hbar = 3L_T$ (Figure 2e). This yields a power law $\delta h_{mix}^{-1} = 0.78 Pe_{L_T}^{-0.28}$, similar to equation (9). Resemblance of both results is more evident from a boxplot comparison (Figure 2f), particularly for Pe in the range of 10^1–10^3.

4. Discussion

This study investigated the dynamics of bioconvective MLs in Lake Cadagno, over a period of six field campaigns. The average h_{mix} was 0.61 ± 0.30 m associated with a mean convective time scale of $\tau_* \approx 23$ min (where $\tau_* = \left(h_{mix}^2/J_b\right)^{1/3}$). To quantify the interplay between convection and diffusion, we compare the rate of ML smoothing with the convective velocity. Given a background diffusivity of $K_{W94} = 1.6 \times 10^{-6}$ m^2 s^{-1} (in agreement with our average result), the time scale required to smooth out a 1.2 m ($\overline{h} = \overline{h_{mix}} + 4\overline{\delta}$) inactive ML is only 2.5 hr (i.e., when $h_{mix} = \delta$, hence $\tau = h^2/100K$; Figure S1c). This yields a ML smoothing rate of $u_K \approx 0.13$ mm s^{-1}. In comparison, the estimated average convective plume velocity w_* is 0.46 ± 0.37 mm s^{-1}. Observed conditions of $w_* > u_K$ explain the maintenance of the convective ML. Moreover, it demonstrates that convection generated by bacteria should be quasi-continuous or else diffusion would smooth out the MLs within ~2.5 hr. This implies that, although present photoautotrophic bacteria rely on sunlight, they need to remain actively moving also during nights, which last much longer than 2.5 hr. Although less intense during night, dissipation is still not negligible ($\varepsilon_{ML}^{night} = 4.0 \times 10^{-10}$ W kg^{-1} ⟨2.8⟩; $\varepsilon_{ML}^{night}/\varepsilon_{ML}^{day} \approx 0.5$), which supports a quasi-continuous bacterial swimming activity.

Whether measured MLs exhibit instantaneous active convection cannot be assessed with the Φ_T shape model. To maintain a homogeneous ML, convective mixing has to overcome the smoothing effects of background diffusivity, that is, $J_b^{ML} \geq J_b^B$. Using microstructure measurements, we further estimated the background buoyancy flux as $J = KN_B^2$. A χ_Θ-based buoyancy flux (Monismith et al., 2018) yields the following condition:

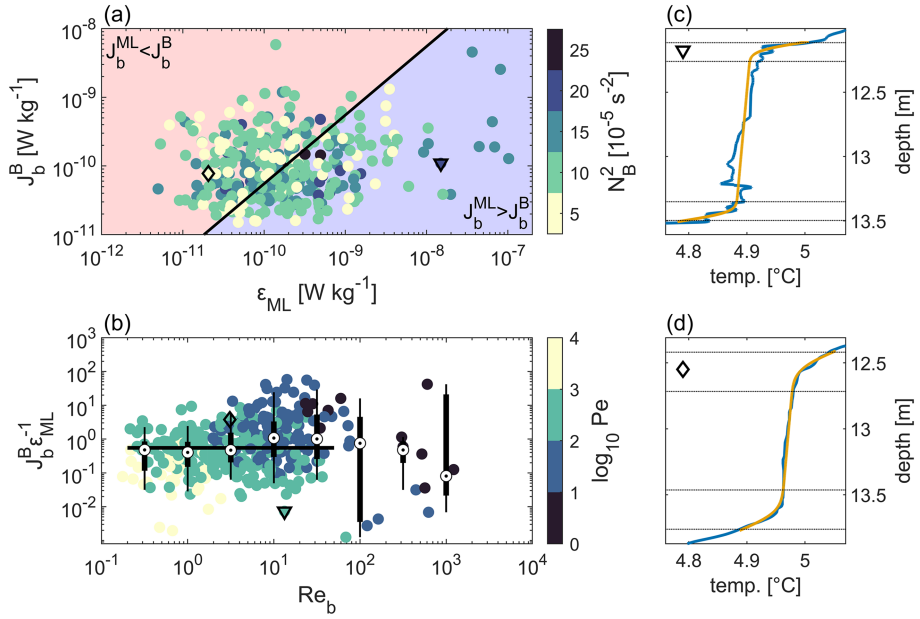

Figure 3. Activity condition for buoyancy fluxes. (a) χ_θ-based background buoyancy flux as a function of ε_{ML}, color-coded according to background stability N_B^2. The thick black line represents the relation $J_b^B = 0.55\varepsilon_{ML}$. (b) $J_b^B\varepsilon_{ML}^{-1}$ as a function of background Re_b, with a Péclet number (Pe) color bar. Dotted white circles represent the median of buoyancy fluxes for half-decade Re_b bins. Black vertical bars and lines represent 75% and 95% confidence intervals for each bin, respectively. The black horizontal line denotes the convective mixing efficiency $\eta_{bC} = 0.55$ used in this study. (c and d) Examples of measured MLs (blue) accompanied by its respective Φ_T fitting (yellow). Segments between dotted lines, represent 2δ. These examples are noted in (a) and (b) by the symbols ▽ and ◇, respectively.

$$J_b^{ML} = \eta_{bC}\,\varepsilon_{ML} \geq \frac{\chi_\theta}{2\left(\frac{\partial T}{\partial z}\right)^2} N_B^2 = J_b^B, \tag{10}$$

where the background χ_θ is obtained from the Batchelor fitting procedure (together with ε_B) and $\frac{\partial T}{\partial z}$ is the background temperature gradient. J_b^B is presented in Figure 3a as a function of ε_{ML} and compared with the relation $J_b^{ML} = 0.55\varepsilon_{ML}$ (black line; equation (4)). This comparison shows that 49% of the observed MLs do not fulfill the activity condition imposed by equation (10). The relation used may be representative of active MLs only, yet an average mixing efficiency of 0.55 for the range $Re_b < 10$ (Figure 3b) represents a realistic approximation. Figures 3c and 3d show examples that respectively fulfill or violate condition (10), depicting different MLs for relatively similar J_b^B conditions. Sharp MLs (Figure 3c) could be due to active convection whereas smooth MLs (Figure 3d) to decaying convective turbulence. Therefore, we suggest that cases not fulfilling equation (10) could be related to reduced bacterial migration.

Convective-diffusive systems and their specific mixing efficiency remain poorly investigated at field scale in natural waters. Although this study focuses on in situ characterization of biologically driven MLs, findings presented in Figure 3 could also constrain hydrodynamic parameters for modeling (bio)convection.

We characterized the competition between convection and turbulent diffusion using two different approximations. The first consists of estimating bulk ML properties by fitting temperature profiles to a diffusive-shape model. The second is dynamic, and microstructure measurements are used to estimate instantaneous dissipations and buoyancy fluxes in the ML and its surroundings. In general, convection dominates; however, the measurements present a nonnegligible variability (Figures 2d–2f and 3). This can be explained by an irregular injection of energy to the system (internal waves weakly energized by wind forcing; Figure S2), nonconstant bacterial migration, and the intermittent nature of turbulence. Altogether, the results suggest that dynamic characteristics can be estimated from ML shape properties (and vice versa; equation (9)).

To generalize our results, we investigated whether turbulent estimates can be obtained from varying macroscopic parameters (i.e., $\delta h_{\mathrm{mix}}^{-1}$) of other systems exhibiting convectively driven MLs. Using data from double-diffusive staircases in Lake Kivu (Sommer, Carpenter, Schmid, Lueck, Schurter, & Wüest, 2013) and analyzing a microstructure profile with the ML model Φ_T (equation (3) and Figure S5) gives $\overline{\delta h_{\mathrm{mix}}^{-1}} = 0.08$ (Sommer, Carpenter, Schmid, Lueck, Schurter, & Wüest, 2013, reported $\overline{h_T} = \overline{2\delta} = 0.09$ m and $\overline{H_T} = \overline{h_{\mathrm{mix}}} = 0.70$ m to give a $\overline{\delta h_{\mathrm{mix}}^{-1}} = 0.07$). Applying equation (9) yields $Pe = 3.4 \times 10^3$, and thus, $J_{\mathrm{b}}^{Pe} = 3.1 \times 10^{-10}$ W kg^{-1}. Recently, Sommer et al. (2019) reported an average dissipation within the MLs of Lake Kivu of 1.5×10^{-10} W kg^{-1}. The same study considers a mixing efficiency of 0.8, and thus, a $J_{\mathrm{b}} = 1.9 \times 10^{-10}$ W kg^{-1}, which is in good agreement with J_{b}^{Pe}.

We also analyzed data from under-ice convection in Lake Onega (Bouffard et al., 2016, 2019). Mooring measurements during radiative daytime hours in March 2016 (Figure S6a) indicate a ML with an average $\overline{\delta h_{\mathrm{mix}}^{-1}} = 0.08$ ($\overline{\delta} = 0.66$ m and $\overline{h_{\mathrm{mix}}} = 8.3$ m). This combines with equation (9) to give $Pe = 3.5 \times 10^3$. A known buoyancy flux for under-ice convection, determined from the radiative forcing (Ulloa et al., 2018), allows us to estimate diffusivity using the scaling described here. The average $J_{\mathrm{b}} = 3.6 \times 10^{-10}$ W kg^{-1} (Figure S6a; $w_* = 1.4$ mm s^{-1}) thus gives a bulk diffusivity of $K_{\mathrm{B}}^{Pe} = 3.4 \times 10^{-6}$ m^2 s^{-1}. This value coincides with an independent microstructure profiler-based estimate of 1.4×10^{-6} m^2 s^{-1} (measured the same day; Figures S6b and S6c).

Bulk turbulent parameters estimated using the proposed methods show good agreement with independent observations of double-diffusion in Lake Kivu and under-ice convection in Lake Onega. Moreover, the non-symmetric ML model showed good potential for analyzing surface convective MLs in Lake Geneva (Figure S3). Therefore, a data-based Péclet number scaling of convection-diffusion competition could be considered to estimate bulk turbulent parameters of other convective processes, such as cooling-induced surface convection (Shay & Gregg, 1986; Tedford et al., 2014) and thermobaric convection (Crawford & Collier, 1997; Schmid et al., 2008).

5. Conclusions

In this study, we focused on the competition between convection and turbulent diffusion in stratified natural waters. The bioconvection observed during six field campaigns in the strongly stratified Lake Cadagno (Switzerland) offers an ideal environment for this analysis with the following conclusions:

1. Dense and heavy motile photoautotrophic bacteria are able to convectively homogenize a meter-scale layer against the omnipresent effect of shear-induced eddy diffusion as typical in stratified lakes. The presented analysis allows comparing the competing effects of convection and turbulent diffusion and thereby allows drawing conclusions on biological activities purely based on physical profile information.
2. Bioconvective mixed layers (MLs), which consistently form in the interior of the strongly stratified water body, were analyzed using a diffusive-shape ML model. This approach allowed us to estimate ML thickness (h_{mix}) as well as the extent of the transition to background stratification influenced by (turbulent) diffusive processes (δ) and thereby to characterize the competition between convection and (turbulent) diffusion.
3. The combined ML shape (h_{mix} and δ) and Péclet number scaling yields bulk estimates of the ML buoyancy flux and background diffusivity. The generalization of this scheme showed good agreement with double-diffusive and under-ice radiatively driven convection in other aquatic systems.

Data

Field measurements used in this research are available online (https://doi.org/10.5281/zenodo.3507638).

Acknowledgments
We thank Piora Centro Biologia Alpina (CBA) for use of the sampling platform and housing. We are indebted to our technical staff, Sébastien Lavanchy (EPFL) and Michael Plüss (Eawag), for logistics and support in the field and to Tobias Sommer for guidance in VMP operation. We also thank SUPSI colleagues: Samuele Roman (also CBA), Francesco Danza, Nicola Storelli, and Samuel Lüdin and EPFL/Eawag interns and colleagues: Angelo Carlino, Emilie Haizmann, Oliver Truffer, Hannah Chmiel, Cintia Ramón Casañas, Love Råman Vinnå, and Tomy Doda for their assistance during fieldwork. Hugo N. Ulloa, Bieito Fernández-Castro, Kraig Winters, Cary Troy, and Alex Forrest provided helpful discussions on convective processes. Constructive criticism from two anonymous reviewers improved this manuscript.

This work was financed by the Swiss National Science Foundation Sinergia Grant CRSII2_160726 (A Flexible Underwater Distributed Robotic System for High-Resolution Sensing of Aquatic Ecosystems). There are no financial conflicts of interests for any author.

References

Baker, M. A., & Gibson, C. H. (1987). Sampling turbulence in the stratified ocean: Statistical consequences of strong intermittency. *Journal of Physical Oceanography*, *17*(10), 1817–1836. https://doi.org/10.1175/1520-0485(1987)017<1817:STITSO>2.0.CO;2

Batchelor, G. K. (1959). Small-scale variation of convected quantities like temperature in turbulent fluid. Part 1. General discussion and the case of small conductivity. *Journal of Fluid Mechanics*, *5*(1), 113–133. https://doi.org/10.1017/S002211205900009X

Bouffard, D., Boegman, L., & Rao, Y. R. (2012). Poincaré wave–induced mixing in a large lake. *Limnology and Oceanography*, *57*(4), 1201–1216. https://doi.org/10.4319/lo.2012.57.4.1201

Bouffard, D., & Wüest, A. (2019). Convection in lakes. *Annual Review of Fluid Mechanics*, *51*(1), 189–215. https://doi.org/10.1146/annurev-fluid-010518-040506

Bouffard, D., Zdorovennov, R. E., Zdorovennova, G. E., Pasche, N., Wüest, A., & Terzhevik, A. Y. (2016). Ice-covered Lake Onega: Effects of radiation on convection and internal waves. *Hydrobiologia*, *780*(1), 21–36. https://doi.org/10.1007/s10750-016-2915-3

Bouffard, D., Zdorovennova, G., Bogdanov, S., Efremova, T., Lavanchy, S., Palshin, N., et al. (2019). Under-ice convection dynamics in a boreal lake. *Inland Waters*, *9*(2), 142–161. https://doi.org/10.1080/20442041.2018.1533356

Crawford, G. B., & Collier, R. W. (1997). Observations of a deep-mixing event in Crater Lake, Oregon. *Limnology and Oceanography*, *42*(2), 299–306. https://doi.org/10.4319/lo.1997.42.2.0299

Dillon, T. M. (1982). Vertical overturns: A comparison of Thorpe and Ozmidov length scales. *Journal of Geophysical Research*, *87*(C12), 9601–9613. https://doi.org/10.1029/JC087iC12p09601

Gibson, C. H. (1980). Fossil temperature, salinity, and vorticity turbulence in the ocean. In J. C. Nihoul (Ed.), *Marine Turbulence Proceedings of the 11th International Liege Colloquium on Ocean Hydrodynamics*, *Elsevier Oceanography Series* (Vol. 28, pp. 221–257). New York NY: Elsevier/North-Holland Inc. https://doi.org/10.1016/S0422-9894(08)71223-6

Huppert, H. E., & Turner, J. S. (1972). Double-diffusive convection and its implications for the temperature and salinity structure of the ocean and Lake Vanda. *Journal of Physical Oceanography*, *2*(4), 456–461. https://doi.org/10.1175/1520-0485(1972)002<0456:DDCAII>2.0.CO;2

Imberger, J. (1985). The diurnal mixed layer. *Limnology and Oceanography*, *30*(4), 737–770. https://doi.org/10.4319/lo.1985.30.4.0737

Ivey, G. N., Winters, K. B., & Koseff, J. R. (2008). Density stratification, turbulence, but how much mixing? *Annual Review of Fluid Mechanics*, *40*(1), 169–184. https://doi.org/10.1146/annurev.fluid.39.050905.110314

Kirillin, G., Leppäranta, M., Terzhevik, A., Granin, N., Bernhardt, J., Engelhardt, C., et al. (2012). Physics of seasonally ice-covered lakes: A review. *Aquatic Sciences*, *74*(4), 659–682. https://doi.org/10.1007/s00027-012-0279-y

Lombardo, C. P., & Gregg, M. C. (1989). Similarity scaling of viscous and thermal dissipation in a convecting surface boundary layer. *Journal of Geophysical Research*, *94*(C5), 6273–6284. https://doi.org/10.1029/JC094iC05p06273

Lorke, A., Peeters, F., & Wüest, A. (2005). Shear-induced convective mixing in bottom boundary layers on slopes. *Limnology and Oceanography*, *50*(5), 1612–1619. https://doi.org/10.4319/lo.2005.50.5.1612

Monismith, S. G., Koseff, J. R., & White, B. L. (2018). Mixing efficiency in the presence of stratification: When is it constant? *Geophysical Research Letters*, *45*, 5627–5634. https://doi.org/10.1029/2018GL077229

Moum, J. N., Perlin, A., Klymak, J. M., Levine, M. D., Boyd, T., & Kosro, P. M. (2004). Convectively driven mixing in the bottom boundary layer. *Journal of Physical Oceanography*, *34*(10), 2189–2202. https://doi.org/10.1175/1520-0485(2004)034<2189:CDMITB>2.0.CO;2

Osborn, T. R. (1980). Estimates of the local rate of vertical diffusion from dissipation measurements. *Journal of Physical Oceanography*, *10*(1), 83–89. https://doi.org/10.1175/1520-0485(1980)010<0083:EOTLRO>2.0.CO;2

Ruddick, B., Anis, A., & Thompson, K. (2000). Maximum likelihood spectral fitting: The batchelor spectrum. *Journal of Atmospheric and Oceanic Technology*, *17*(11), 1541–1555. https://doi.org/10.1175/1520-0426(2000)017<1541:MLSFTB>2.0.CO;2

Saggio, A., & Imberger, J. (2001). Mixing and turbulent fluxes in the metalimnion of a stratified lake. *Limnology and Oceanography*, *46*(2), 392–409. https://doi.org/10.4319/lo.2001.46.2.0392

Sánchez, X., & Roget, E. (2007). Microstructure measurements and heat flux calculations of a triple-diffusive process in a lake within the diffusive layer convection regime. *Journal of Geophysical Research*, *112*, C02012. https://doi.org/10.1029/2006JC003750

Schanz, F., Fischer-Romero, C., & Bachofen, R. (1998). Photosynthetic production and photoadaptation of phototrophic sulfur bacteria in Lake Cadagno (Switzerland). *Limnology and Oceanography*, *43*(6), 1262–1269. https://doi.org/10.4319/lo.1998.43.6.1262

Schmid, M., Budnev, N. M., Granin, N. G., Sturm, M., Schurter, M., & Wüest, A. (2008). Lake Baikal deepwater renewal mystery solved. *Geophysical Research Letters*, *35*, L09605. https://doi.org/10.1029/2008GL033223

Shay, T. J., & Gregg, M. C. (1986). Convectively driven turbulent mixing in the upper ocean. *Journal of Physical Oceanography*, *16*(11), 1777–1798. https://doi.org/10.1175/1520-0485(1986)016<1777:CDTMIT>2.0.CO;2

Sommer, T., Carpenter, J. R., Schmid, M., Lueck, R. G., Schurter, M., & Wüest, A. (2013). Interface structure and flux laws in a natural double-diffusive layering. *Journal of Geophysical Research: Oceans*, *118*, 6092–6106. https://doi.org/10.1002/2013JC009166

Sommer, T., Carpenter, J. R., Schmid, M., Lueck, R. G., & Wüest, A. (2013). Revisiting microstructure sensor responses with implications for double-diffusive fluxes. *Journal of Atmospheric and Oceanic Technology*, *30*(8), 1907–1923. https://doi.org/10.1175/JTECH-D-12-00272.1

Sommer, T., Danza, F., Berg, J., Sengupta, A., Constantinescu, G., Tokyay, T., et al. (2017). Bacteria-induced mixing in natural waters. *Geophysical Research Letters*, *44*, 9424–9432. https://doi.org/10.1002/2017GL074868

Sommer, T., Schmid, M., & Wüest, A. (2019). The role of double diffusion for the heat and salt balance in Lake Kivu. *Limnology and Oceanography*, *64*(2), 650–660. https://doi.org/10.1002/lno.11066

Steinbuck, J. V., Stacey, M. T., & Monismith, S. G. (2009). An Evaluation of χ_T estimation techniques: Implications for Batchelor fitting and ε. *Journal of Atmospheric and Oceanic Technology*, *26*(8), 1652–1662. https://doi.org/10.1175/2009JTECHO611.1

Tedford, E. W., MacIntyre, S., Miller, S. D., & Czikowsky, M. J. (2014). Similarity scaling of turbulence in a temperate lake during fall cooling. *Journal of Geophysical Research: Oceans*, *119*, 4689–4713. https://doi.org/10.1002/2014JC010135

Thorpe, S. A. (1977). Turbulence and mixing in a Scottish Loch. *Philosophical Transactions of the Royal Society A: Mathematical, Physical and Engineering Sciences*, *286*(1334), 125–181. https://doi.org/10.1098/rsta.1977.0112

Uhde, M. (1992). Mischungsprozesse im Hypolimnion des mero- miktischen lago Cadagno: Eine Untersuchung mit Hilfe natürlicher und künstlicher Tracer. Master Thesis, University of Freiburg, Germany.

Ulloa, H. N., Wüest, A., & Bouffard, D. (2018). Mechanical energy budget and mixing efficiency for a radiatively heated ice-covered waterbody. *Journal of Fluid Mechanics*, *852*, R1. https://doi.org/10.1017/jfm.2018.587

Wüest, A. (1994). Interactions in lakes: Biology as source of dominant physical forces. *Limnologica*, *24*(2), 93–104.

Wüest, A., Piepke, G., & Van Senden, D. C. (2000). Turbulent kinetic energy balance as a tool for estimating vertical diffusivity in wind-forced stratified waters. *Limnology and Oceanograhy*, *45*(6), 1388–1400. https://doi.org/10.4319/lo.2000.45.6.1388

Yang, B., Young, J., Brown, L., & Wells, M. (2017). High-frequency observations of temperature and dissolved oxygen reveal under-ice convection in a large lake. *Geophysical Research Letters*, *44*, 12,218–12,226. https://doi.org/10.1002/2017GL075373